THE JOURNAL OF PHYSICAL CHEMISTRY A

Article

Cite This: J. Phys. Chem. A 2019, 123, 6185−6193

pubs.acs.org/JPCA

Isobutane Infrared Bands: Partial Rotational Assignments, ab Initio Calculations, and Local Mode Analysis

Peter F. Bernath,*[,†] Dror M. Bittner,[†] and Edwin L. Sibert III[‡]

[†]Department of Chemistry and Biochemistry, Old Dominion University, Norfolk, Virginia 23529, United States

[‡]Department of Chemistry, University of Wisconsin—Madison, Madison, Wisconsin 53706, United States

Supporting Information

ABSTRACT: High-resolution infrared spectra of the symmetric top isobutane $CH(CH_3)_3$ were assigned with the help of ab initio calculations. The strong parallel band $\nu_5(a_1)$ with an origin at 1396.54741(76) cm^{-1} and the $\nu_4(a_1)$ mode, the CH_2 scissors, at 1478.20363(41) cm^{-1} were rotationally analyzed. The bands in the C−H stretching region were assigned with the help of an anharmonic calculation and a local mode analysis.

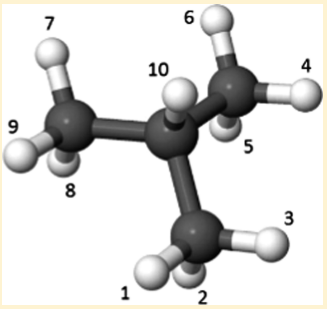

INTRODUCTION

Isobutane and other volatile organic compounds (VOCs) are present in the Earth's atmosphere.[1,2] Emission from oil and gas production is an important source of nonmethane hydrocarbons.[3] For isobutane, anthropogenic emissions are the only source, with biomass burning and biogenic and oceanic emissions estimated to be negligible.[1] These VOCs are oxidized by OH and result in tropospheric ozone pollution in the presence of NO_x (NO and NO_2).

Butane (C_4H_{10}) is also likely an astronomical molecule formed in the atmosphere of Titan[4] and Saturn.[5] Titan, the largest moon of Saturn, has an atmosphere of N_2 and CH_4, which results in the photochemical formation of numerous hydrocarbons.[4] Dobrijevic et al.[4] predict that the abundance of butane on Titan is similar to that of propane, which has already been detected.[6] Butane is predicted to be the most abundant C_4 hydrocarbon on Saturn[5] where propane has also been detected.[7]

Butane has two isomers, *n*-butane with C_{2h} symmetry at equilibrium[8] and isobutane with C_{3v} symmetry at equilibrium.[9] We have recorded high-resolution spectra of isobutane at low temperatures (~200−295 K) in the 3 μm region[10] and 1050−1900 cm^{-1} [11] with N_2 and H_2 as broadening gases. The goal of this latter work was to provide high-resolution infrared absorption cross sections for the detection of isobutane on Titan and Saturn. It turned out that with the new data we can improve the analysis of the infrared spectra and two of the bands had analyzable rotational structure. This work, following refs 10 and 11, is our third paper on isobutane and reports on the rotational and vibrational analyses.

Isobutane has a small dipole moment of 0.132 D,[9] and its microwave[12] and millimeter-wave[13] spectra have been measured. A molecular structure was derived by Hilderbrandt and Wieser, combining electron diffraction and microwave data.[14]

Isobutane has 24 fundamental vibrational frequencies, 8 with a_1 symmetry, 4 optically forbidden a_2 modes (ν_9−ν_{12}), and 12 doubly degenerate e modes (ν_{13}−ν_{24}). The vibrational analysis began in 1946 with the partial assignment of the infrared and Raman spectra to calculate the entropy.[15] Bernstein and co-workers provided a more thorough vibrational analysis of isobutane and deuterated isobutane.[16,17] In 1963, Schachtschneider and Snyder carried out a force field analysis.[18] The torsional frequencies ($\nu_{12}(a_1)$ 225 cm^{-1}, $\nu_{24}(e)$ 280 cm^{-1}) and the barrier to internal rotation of the methyl groups (~1400 cm^{-1}) were determined by Weiss and Leroi.[19] A partial assignment of the C−H fundamentals and C−H overtones was obtained from a local mode analysis.[20] Spectra of C−H overtones were also measured by photoacoustic spectroscopy.[21] Matrix-isolated infrared spectra are available.[22] Recent Raman spectra were recorded in high-pressure CH_4.[23]

In addition to force field calculations, ab initio harmonic calculations of isobutane vibrational frequencies and intensities have been published. Manzanares et al. carried out scaled HF/6-31G* calculations,[20] and more recently, an MP2/6-31G* calculation was published by Mirkin and Krimm.[24] Anharmonic frequency calculations are possible, and, for example, Gerber and co-workers have used the vibrational self-consistent field method with the second-order perturbation theory to calculate the C−H stretching modes of *n*-butane (but not isobutane).[25]

The C−H modes of hydrocarbons are very anharmonic and perturbed by Fermi (F) resonance with CH_2 first overtones

Received: April 9, 2019
Revised: June 28, 2019
Published: June 28, 2019

Downloaded via OLD DOMINION UNIV on July 6, 2020 at 21:12:18 (UTC).
See https://pubs.acs.org/sharingguidelines for options on how to legitimately share published articles.

© 2019 American Chemical Society

DOI: 10.1021/acs.jpca.9b03321
J. Phys. Chem. A 2019, 123, 6185−6193

and combination modes of CH_2 scissor vibrations.[26] In recent years, Zwier and co-workers have studied the spectra of allyl benzene by infrared−ultraviolet double resonance, focusing on assignments of the C−H stretching modes.[27] Sibert and co-workers have modeled the C−H stretching region with a local mode model that includes the CH_2 bending Fermi resonance interactions.[28] The C−H region is an important probe of conformation and environment in biological systems.

EXPERIMENTAL SECTION

High-resolution infrared spectra of isobutane have been used for the analysis. The spectra were measured at the Canadian light source (CLS) far-infrared beamline. A more detailed description of the experiment can be found elsewhere.[10,11] In brief, the spectra were recorded using a Bruker IFS 125 HR Fourier transform spectrometer. As the spectra were intended to be used for absorption cross sections, pure samples of isobutane and isobutane with three different pressures of N_2 and H_2 at four temperatures were recorded (~200−295 K).

In the 2500−3300 cm^{-1} region, the spectrum of isobutane at 203 K with 100 Torr of N_2 recorded with a 0.04 cm^{-1} spectral resolution[10] was used because it had the best signal-to-noise ratio (Figure 1). The rotational structure was not clearly

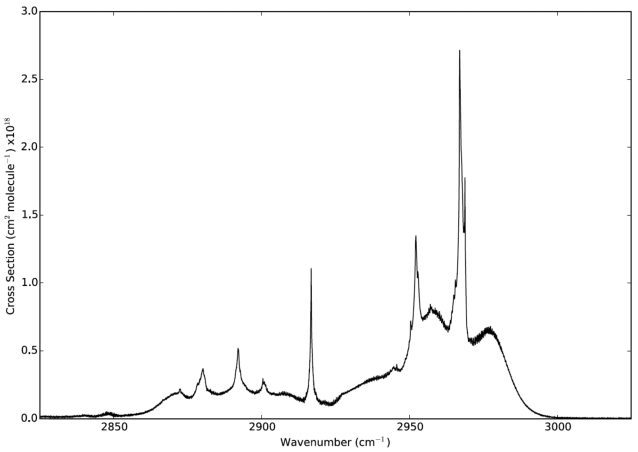

Figure 1. Isobutane absorption cross sections at 0.04 cm^{-1} resolution in the 3.3 μm region[9] at 203 K with 100 Torr of N_2.

resolved. In the 1050−1900 cm^{-1} spectral range[10] (Figure 2), isobutane at 210 K with 10 Torr of N_2 recorded at 0.005 cm^{-1} resolution was used. In this case, the rotational structure was resolved more clearly in the pure spectrum but with a poorer signal-to-noise ratio. The spectrum selected had the best signal-to-noise ratio with a clear rotational structure.

An infrared spectrum of isobutane at 5 °C from the Pacific Northwest National Laboratory (PNNL) infrared database was also used.[29] This spectrum was recorded at 0.1 cm^{-1} resolution from 600 to 6500 cm^{-1} with 1 atm of N_2 broadening gas at 5 °C.

AB INITIO CALCULATIONS

Harmonic and anharmonic vibrational frequencies have been calculated using Gaussian 09 electronic structure package.[30] Harmonic frequencies have been calculated at the MP2/aug-cc-pVTZ and B3LYP/aug-cc-pVQZ levels of theory. Anharmonic frequencies have been calculated at the MP2/aug-cc-pVTZ level of theory. The local mode model, to be described

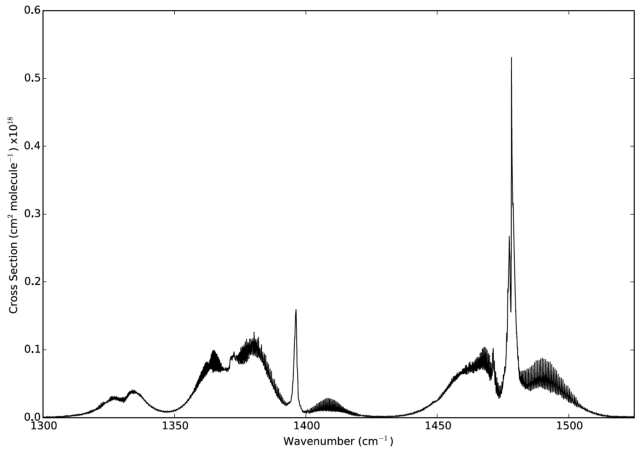

Figure 2. Isobutane absorption cross sections[10] from 1300 to 1525 cm^{-1} with 0.005 cm^{-1} resolution at 210 K with 10 Torr of N_2.

below, uses harmonic frequencies calculated at the B3LYP/6-311++(d,p) and CCSD(T)/cc-pVTZ levels of theory.

LOCAL MODE MODEL

The local mode model reported in this work is described in the work of Tabor et al.[28] In this section, we present the salient features as they apply to isobutane. The key steps are to determine the Hamiltonian describing the local mode CH stretches and scissor modes at the harmonic level. The diagonal elements of the corresponding Hamiltonian matrix are scaled according to previously determined scale factors.[28] We then added Fermi couplings between the CH stretches with the overtones and combination bands of the scissors. These couplings and other select anharmonic couplings, which are assumed to be transferrable, have been obtained from simple model systems.[28]

The local mode Hamiltonian consists of 19 degrees of freedom. The stretch contribution to the Hamiltonian consists of 10 CH stretches r_n, where n corresponds to the associated H atoms labeled in Figure 3. The scissor contribution consists of

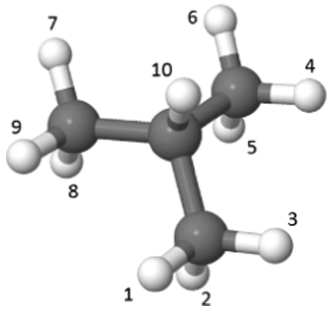

Figure 3. Isobutane structure and numbering scheme for local mode analysis.

the nine scissor modes, three for each methyl group. The scissor coordinates are labeled by the H atom not involved in the motion. For example, ϕ_3 corresponds to the H_1CH_2 scissor mode. Collectively, these coordinates are described by the vector $\boldsymbol{R} = \{r_1,..., r_{10}, \varphi_1,..., \varphi_9\}$.

We obtain the localized coordinates directly from the normal coordinates $\boldsymbol{Q}$ via an orthogonal transformation, $\boldsymbol{R} = \boldsymbol{AQ}$. The transformation matrix $\boldsymbol{A}$ is determined in several steps. Using the stretches as an example, we find a localized mode

DOI: 10.1021/acs.jpca.9b03321
J. Phys. Chem. A 2019, 123, 6185−6193

associated with the CH_i stretch by carrying out a normal mode calculation in which all of the H atom masses are increased by a factor c, save for the mass of atom i, which retains its original value. One of the resulting normal modes, Q_i', corresponds to a vibration localized on the CH_i stretch. The process is repeated for each of the 10 stretches to find 10 CH-localized normal modes, $\boldsymbol{Q}'$. These modes are expressed as linear combinations of the 10 original normal coordinates $\boldsymbol{Q}' = \boldsymbol{LQ}$ with minor contributions from lower-frequency modes.

Since the rows of $\boldsymbol{L}$ are calculated from distinct normal mode calculations, this matrix is not orthogonal. It can be well approximated as an orthogonal matrix as follows. Calculating the overlap $\boldsymbol{S} = \boldsymbol{L}^{\mathrm{T}}\boldsymbol{L}$ and solving for $\boldsymbol{S}^{-1/2}$, we find the desired localized coordinates $\boldsymbol{R} = \boldsymbol{LS}^{-1/2}\boldsymbol{Q} \equiv \boldsymbol{AQ}$ that describe the CH stretch vibrations. The resulting Hamiltonian is

$$H = \frac{1}{2}\sum_{i=1}^{10} P_i^2 + \frac{1}{2}\sum_{i=1}^{10} F_{ij}R_iR_j \tag{1}$$

where the F_{ij} elements are obtained by transforming the Hessian obtained from electronic structure calculations. If the normal mode force constants are given as f_{ii}, then $\boldsymbol{F} = \boldsymbol{AfA}^{\mathrm{T}}$.

The $\boldsymbol{F}$ matrix has three important properties: (1) it includes off-diagonal couplings between the stretches, due to the localization of the modes, (2) there are no elements coupling the stretches to the remaining degrees of freedom, and (3) if you diagonalized the $\boldsymbol{F}$ matrix, you obtain the normal modes. We employ the same procedure for the scissor degrees of freedom.

To obtain the local mode Hamiltonian matrix, we express the Hamiltonian of eq 1 in terms of raising and lowering operators associated with the local modes. We make the approximation that only nearly degenerate local mode states can couple, i.e.

$$R_iR_j = C_iC_j(a_i^\dagger + a_i)(a_j^\dagger + a_j) \approx C_iC_j(a_i^\dagger a_j + a_j^\dagger a_j) \tag{2}$$

Here, the C_i are the standard scaling factors. The resulting lower-left contribution to the Hamiltonian matrix, corresponding to states with one quantum of excitation in each of the CH stretches, is

$$H^{\mathrm{s}} = \begin{pmatrix}
\omega_{\mathrm{A}} & & & & & & & & & \\
V_{\mathrm{AB}} & \omega_{\mathrm{B}} & & & & & & & & \\
V_{\mathrm{AA}} & V_{\mathrm{AB}} & \omega_{\mathrm{A}} & & & & & & & \\
 & & V_{\mathrm{AA}'} & \omega_{\mathrm{A}} & & & & & & \\
 & V_{\mathrm{BB}'} & & V_{\mathrm{AB}} & \omega_{\mathrm{B}} & & & & & \\
 & & & V_{\mathrm{AA}} & V_{\mathrm{AB}} & \omega_{\mathrm{A}} & & & & \\
 & & & & & V_{\mathrm{AA}'} & \omega_{\mathrm{A}} & & & \\
 & V_{\mathrm{BB}'} & & & V_{\mathrm{BB}'} & & V_{\mathrm{AB}} & \omega_{\mathrm{B}} & & \\
V_{\mathrm{AA}'} & & & & & & V_{\mathrm{AA}} & V_{\mathrm{AB}} & \omega_{\mathrm{A}} & \\
V_{\mathrm{AC}} & V_{\mathrm{BC}} & V_{\mathrm{AC}} & V_{\mathrm{AC}} & V_{\mathrm{BC}} & V_{\mathrm{AC}} & V_{\mathrm{AC}} & V_{\mathrm{BC}} & V_{\mathrm{AC}} & \omega_{\mathrm{C}}
\end{pmatrix} \tag{3}$$

The elements of $\boldsymbol{H}^{\mathrm{s}}$ elements whose magnitudes are less than 1 cm^{-1} are not shown. Table 1 provides numerical values for the matrix elements for two different levels of theory. There are several features to note that are common to both calculations. The diagonal elements, associated with the CH methyl stretches, have two possible values. We differentiate between them using A and B subscripts. From Figure 3, one can see that modes 2, 5, and 8, denoted with a B subscript, are all antiparallel to the lone CH, denoted with a C subscript. There are only six relevant, unique coupling values. We use subscripts to distinguish the kinds of modes that are being coupled. The V_{AB} coupling represents the coupling between modes of types A and B on the same methyl. If the coupling is between CH stretch on different methyl groups, a prime is added to the subscript. Interestingly, there are only two types of couplings between the CH stretches of different methyl groups that are significant. We note that these results are insensitive to the choice of mass scaling; varying the scaling factor c from 1.4 to 2.4 changes the results by less than 0.1 cm^{-1}. The eigenvalues of the matrix $\boldsymbol{H}^{\mathrm{s}}$ can be compared to the normal mode frequencies reported in Gaussian[30] (in wavenumbers). At the two levels of theory reported in Table 1, the eigenvalues agree to within 0.3 cm^{-1} with the Gaussian CH frequency results. The results are similar but not the same, due to the approximation of eq 2.

Table 1. Matrix Elements for the Stretch, Equation 3, and Scissor, Equation 4, Hamiltonians in cm^{-1}

	level of theory 1[a]	level of theory 2[b]
stretch element		
ω_{A}	3059.1	3077.4
ω_{B}	3042.4	3061.1
ω_{C}	2997.2	3024.9
V_{AB}	−20.5	−24.3
V_{BB}	−20.4	−24.4
$V_{\mathrm{BB}'}$	2.0	1.4
$V_{\mathrm{AA}'}$	2.6	1.8
V_{AC}	4.8	4.7
V_{BC}	−9.5	−8.5
scissor element		
ω_{D}	1468.7	1473.7
ω_{E}	1469.3	1472.0
V_{DE}	−29.2	−30.8
V_{DD}	−29.1	−30.0
$V_{\mathrm{DD}'}$	11.6	12.4
$V_{\mathrm{EE}'}$	10.3	10.5
$V_{\mathrm{DD}''}$	3.1	0.4

[a]Calculated at the B3LYP/6-311++(d,p) level of theory. [b]Calculated at the CCSD(T)/cc-pVTZ level of theory.

There are several aspects worth noting. The 3 × 3 sub-blocks corresponding to the CH_3 stretches are identical, as expected based on symmetry. The couplings between CH stretches on different methyl groups are small, with the largest coupling magnitude occurring between those CH stretch groups pointing in the same directions, these being the (1,9), (3,4), (6,7), (2,5), (2,8), and (5,8) pairs. The coupling between the lone CH to the methyl CH stretches is substantially stronger. We consider the importance of this coupling below.

The results for the two levels of theory given in Table 1 are in good agreement. The final results use scaled frequencies, the two notable differences are the slightly higher V_{AA} and V_{AB} couplings between CH stretches on the same methyl group found for CCSD(T) and the slightly higher frequency of the lone CH stretch frequency relative to the methyl CH stretches, $\omega_A - \omega_C$ being about 10 cm^{-1} less for the CCSD(T) calculation.

The 9 × 9 scissor Hamiltonian

DOI: 10.1021/acs.jpca.9b03321
J. Phys. Chem. A 2019, 123, 6185−6193

$$H^{b} = \begin{pmatrix} \omega_D & & & & & & & & \\ V_{DE} & \omega_E & & & & & & & \\ V_{DD} & V_{DE} & \omega_D & & & & & & \\ & & V_{DD'} & \omega_D & & & & & \\ & V_{EE'} & & V_{DE} & \omega_E & & & & \\ V_{DD''} & & & V_{DD} & V_{DE} & \omega_D & & & \\ & & V_{DD''} & & & V_{DD'} & \omega_D & & \\ & V_{EE'} & & & V_{EE'} & & V_{DE} & \omega_E & \\ V_{DD'} & & & V_{DD''} & & & V_{DD} & V_{DE} & \omega_D \end{pmatrix} \quad (4)$$

has a similar form to that of $\boldsymbol{H}^{s}$. The bending motion of the lone CH is not included since the frequency of this mode is sufficiently low, 1358 cm^{-1} at the B3LYP/6-311++(d,p) level of theory, that no resonances with the CH stretches occur.

The anharmonic effects allow combination bands and overtones of the scissor modes to couple with the CH stretch states with one quantum of excitation. The harmonic contribution to this Hamiltonian follows from $\boldsymbol{H}^{s}$ and $\boldsymbol{H}^{b}$ expressed in terms of raising and lowering operators of the stretches and scissors as

$$H^{(0)} = \sum_{i=1}^{10}\sum_{j=1}^{10} H_{ij}^{s} a_i^{\dagger} a_j + \sum_{i=1}^{9}\sum_{j=1}^{9} H_{ij}^{b} b_i^{\dagger} b_j \quad (5)$$

The total basis set used to describe the spectral region of the CH stretch fundamentals contains 55 states. The model assumes that one can ignore anharmonic couplings except those that couple states with excitation on the same methyl group. We base this assumption on the small values of the corresponding harmonic terms. The corresponding 9 × 9 matrix describing the states of a methyl group is

$$\boldsymbol{H}^{CH_3} = \begin{pmatrix} \omega_A & & & & & & & & \\ V_{AB} & \omega_B & & & & & & & \\ V_{AA} & V_{AB} & \omega_A & & & & & & \\ F_2 & F_1 & F_1 & 2\omega_D + 2\chi_{ss} & & & & & \\ F_1 & F_2 & F_1 & 2F_{dd} & 2\omega_E + 2\chi_{ss} & & & & \\ F_1 & F_1 & F_2 & 2F_{dd} & 2F_{dd} & 2\omega_D + 2\chi_{ss} & & & \\ F_3 & F_3 & F_4 & \sqrt{2}V_{DE} & \sqrt{2}V_{DE} & 0 & \omega_D + \omega_E & & \\ F_3 & F_4 & F_3 & \sqrt{2}V_{DD} & 0 & \sqrt{2}V_{DD} & V_{DE} & \omega_D + \omega_D & \\ F_4 & F_3 & F_3 & 0 & \sqrt{2}V_{DE} & \sqrt{2}V_{DE} & V_{DE} & V_{DE} & \omega_D + \omega_E \end{pmatrix} \quad (6)$$

The first three states $|100\rangle$, $|010\rangle$, $|001\rangle$ correspond to CH stretches with excitation in modes 1−3, respectively. The next three $|200\rangle$, $|020\rangle$, $|002\rangle$ correspond to scissor overtones with excitation in the bend modes 1−3, respectively. The last three states $|110\rangle$, $|101\rangle$, $|011\rangle$ correspond to scissor combination bands.

The stretches are coupled to the bending states on the same methyl group via Fermi coupling terms. These couplings are denoted F_i. There are four possible Fermi terms, but the most important one, F_1, corresponds to the coupling term $F_1(a_i^{\dagger}b_j b_j + a_i b_j^{\dagger} b_j^{\dagger})/\sqrt{2}$, where $(i \neq j)$. Initially, these terms were calculated via ab initio methods that involved calculating the associated cubic couplings. These contributions were found to be very similar for several molecules.[31] The F_1 values of methyl and methoxy groups were also found to be very similar to the analogous values for Fermi couplings in CH_2 groups.[31] Computing spectra with the ab initio values systematically leads to more Fermi coupling than is observed experimentally, and we have chosen a scaled value of 21 cm^{-1}.[28] The remaining Fermi couplings are similarly scaled. In addition to being quadratically coupled, the scissor overtones and combination bands are coupled via Darling−Dennison (DD) coupling terms $F_{dd}(b_i^{\dagger}b_i^{\dagger}b_j b_j + b_i b_i b_j^{\dagger} b_j^{\dagger})$. We also include a diagonal anharmonicity that shifts the local bend overtones relative to the combination bands by an amount $2\chi_{ss}$. The magnitudes of these terms follow from perturbative studies on the ethane molecule in a localized representation.[31] The Hamiltonians for the methyl groups all have the same form.

The values of these couplings, reported in Table 2, are taken from a previous study of alkylbenzenes.[28] They are assumed to be transferable in the local representation.

Table 2. Values of the Fermi (F) and Darling−Dennison (DD) Couplings (cm^{-1}) Employed in Local Mode Model of Equation 6

F and DD couplings	value
F_1	22.0
F_2	2.5
F_3	5.6
F_4	1.5
χ_{ss}	−4.5
F_{dd}	−2.5

The final model ingredient includes scaling of the density functional theory frequencies. We scale the methyl stretch and bend frequencies by factors of 0.961 and 0.975, respectively. The lone CH is scaled by 0.9655. We chose this value so that the scaled frequency of 2984 cm^{-1} matches the observed CH stretch fundamental of $(CD_3)_3CH$.

To summarize, the local mode model requires a Hessian as input. This Hessian, which describes the harmonic potential in terms of mass-weighted Cartesian coordinates, is transformed via an orthogonal transformation to a localized representation, in which the scissors and stretches are decoupled from each other and from all of the remaining degrees of freedom. The

DOI: 10.1021/acs.jpca.9b03321
J. Phys. Chem. A 2019, 123, 6185−6193

Table 3. Ab Initio Harmonic and Anharmonic Frequencies (in cm^{-1}) and Intensities (in km mol^{-1}) of Isobutane Fundamental Vibrations and Assigned Band Origins (in cm^{-1})

mode	harmonic frequency MP2/AVTZ	intensity MP2/AVTZ	harmonic frequency B3LYP/AVQZ	intensity B3LYP/AVQZ	anharmonic frequency MP2/AVTZ	exp frequency
$\nu_1(a_1)$	3141.08	71.65	3076.89	98.34	3006.17	2968.8?
$\nu_2(a_1)$	3059.26	20.66	3017.99	16.55	2945.03	2916.76
$\nu_3(a_1)$	3052.15	1.27	2990.36	12.00	2884.90	2892.1
$\nu_4(a_1)$	1531.56	18.61	1513.41	18.07	1486.57	1478.20(41)
$\nu_5(a_1)$	1428.74	4.19	1430.20	2.99	1392.69	1396.54(76)
$\nu_6(a_1)$	1217.86	0.04	1212.31	0.09	1187.23	1189.0
$\nu_7(a_1)$	819.78	0.50	795.40	0.49	802.68	797.3[a]
$\nu_8(a_1)$	429.48	0.09	436.44	0.18	431.67	432[b]
$\nu_9(a_2)$	3145.16	0	3076.31	0	3010.50	
$\nu_{10}(a_2)$	1496.50	0	1483.07	0	1453.73	
$\nu_{11}(a_2)$	959.13	0	956.84	0	941.81	944.6?[a]
$\nu_{12}(a_2)$	214.05	0	208.80	0	216.61	225[b]
$\nu_{13}(e)$	3147.33	40.49	3080.62	58.45	3012.14	2967.0?
$\nu_{14}(e)$	3134.45	7.33	3067.10	6.66	2999.92	2944.6?
$\nu_{15}(e)$	3051.10	30.12	3010.32	35.06	2975.10	2952.2
$\nu_{16}(e)$	1522.34	4.19	1508.00	4.15	1477.09	1477.4
$\nu_{17}(e)$	1504.24	0.34	1489.23	0.35	1461.29	1471.2
$\nu_{18}(e)$	1402.57	8.04	1401.24	6.37	1365.36	1372.0
$\nu_{19}(e)$	1364.40	1.90	1361.05	3.49	1328.45	1330.6
$\nu_{20}(e)$	1207.22	1.64	1191.89	2.67	1175.39	1174.3
$\nu_{21}(e)$	994.66	0.08	970.23	0.002	970.81	964.3?[a]
$\nu_{22}(e)$	928.62	0.83	924.35	0.76	917.37	918.7[a]
$\nu_{23}(e)$	362.35	0.03	361.12	0.01	364.43	366[b]
$\nu_{24}(e)$	268.11	0.02	253.28	0.01	263.04	280[b]

[a]From PNNL spectrum. [b]From ref 19.

local diagonal force constants are then scaled. These scalings are taken from previous studies.[28] Anharmonic coupling between the local modes, developed for other systems, is incorporated into the model. Dipoles are calculated ab initio with no adjustments. In this model, all of the interesting differences between the spectra of CH stretch groups reside in the differences that occur at the harmonic level. We assume that the differences between systems, which can lead to dramatically different spectra, are small enough that one can use the same scalings for the harmonic frequencies and the same local anharmonic couplings.

RESULTS AND DISCUSSION

Spectra in the wavenumber ranges of 1050−1900 cm^{-1} (0.005 cm^{-1} resolution, Figure 2), 2500−3300 cm^{-1} (0.04 cm^{-1} resolution, Figure 1), and 600−6500 cm^{-1} (0.1 cm^{-1} resolution) were available. The spectra contain C−C and C−H bending modes and C−C stretches in the 1000−1600 cm^{-1} range and C−H stretches from 2800 to 3100 cm^{-1}. Although the rotational structure was partly resolved for many modes, only two bands [$\nu_4(a_1)$ and $\nu_5(a_1)$] could be rotationally analyzed with the PGOPHER program.[32] For the other bands, the estimated fundamental band origins are provided in Table 3. Table 3 also provides the results of the MP2/aug-cc-pVTZ and B3LYP/aug-cc-pVQZ calculations.

The intense parallel and perpendicular modes were easily distinguished by their band shapes. Parallel transitions had strong Q branches and slightly less intense rotationally resolved P and R branches. Perpendicular transitions generally have weak central features and the lines from sub-bands that spread more-or-less symmetrically from the center. A successful rotational analysis was not achieved for any of the perpendicular bands.

Starting from the lowest-frequency modes, Weiss and Leroi[19] indirectly measured the torsional modes from combination bands [$\nu_{24}(e)$ at 280 cm^{-1} and $\nu_{12}(a_2)$ at 225 cm^{-1}] and directly observed the C−C−C bends $\nu_{23}(e)$ at 366 cm^{-1} and $\nu_8(a_1)$ at 432 cm^{-1}. From the PNNL spectrum, the C−H bends $\nu_7(a_1)$ at 797.3 cm^{-1} and $\nu_{22}(e)$ at 918.7 cm^{-1} are also easily assigned, and all of the directly observed frequencies are within a few cm^{-1} of the anharmonic calculation (Table 1). There is a weak perpendicular mode at 964.3 cm^{-1}, $\nu_{21}(e)$, in the PNNL spectrum (966 cm^{-1} according to Schachtschneider and Snyder).[18] More speculative is the appearance of a nominally forbidden $\nu_{11}(a_2)$ mode at 944.6 cm^{-1} in the PNNL spectrum. These a_2 modes can appear in the spectrum by Coriolis coupling (R_z has a_2 symmetry) with nearby a_1 modes and will therefore have a prominent Q-branch. In fact, the PNNL spectrum has three small sharp features at 943.4 and 944.6 cm^{-1} and very weak 945.9 cm^{-1}, and we have selected the stronger central feature as the a_2 mode.

Switching to the new CLS 1050−1900 cm^{-1} spectrum, the $\nu_{20}(e)$ mode at 1174.3 cm^{-1} is clearly a perpendicular mode, and the very weak nearby a_1 mode is difficult to find. However, there is a small sharp peak at 1189.0 cm^{-1} that is close to the calculated position. The lone C−H bending mode is $\nu_{19}(e)$ at 1330.6 cm^{-1}. The perpendicular mode at 1372.0 cm^{-1} has two central features at 1371.6 and 1372.5 cm^{-1} and is assigned as $\nu_{18}(e)$. The strong parallel band $\nu_5(a_1)$ with an origin at 1396.54741(76) cm^{-1} was rotationally analyzed as was $\nu_4(a_1)$, the CH_2 scissors, at 1478.20363(41) cm^{-1}. There are two weaker features that can tentatively be assigned as $\nu_{17}(e)$ at 1471.2 cm^{-1} and $\nu_{16}(e)$ at 1477.4 cm^{-1}.

DOI: 10.1021/acs.jpca.9b03321
J. Phys. Chem. A 2019, 123, 6185−6193

Two a_1 bands showed a clear rotational structure (Figures 4 and 5) and have been fitted using PGOPHER.[32] The ground-state constants were fixed to the values determined from the millimeter-wave measurements.[13] The bands are perturbed, and effective spectroscopic constants have been determined and are provided in Table 4.

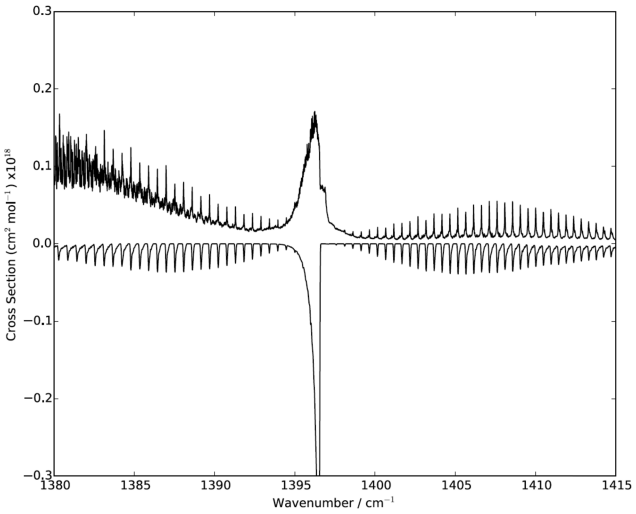

Figure 4. $\nu_5(a_1)$ mode with the PGOPHER simulation pointing downwards.

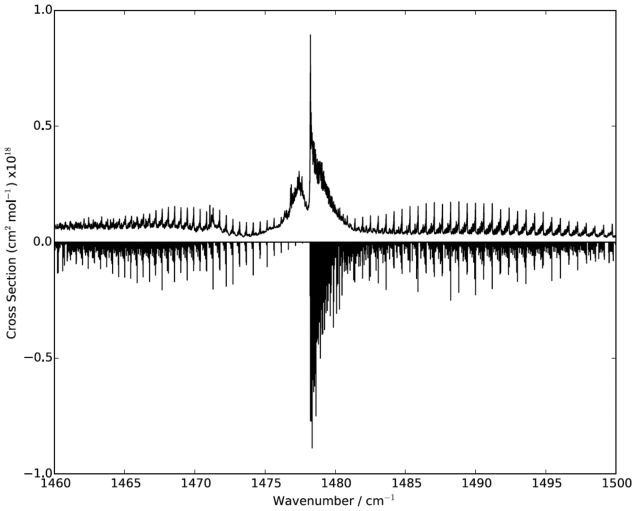

Figure 5. $\nu_4(a_1)$ mode with the PGOPHER simulation pointing downwards.

The assignments of the C−H fundamental modes in the 3.3 μm region are more difficult because the modes are very anharmonic and there are Fermi resonance interactions between the overtone and combination modes of the CH_2 bends near 1470 cm^{-1} and the C−H stretching modes near 2900 cm^{-1}. There are 10 C−H oscillators, 9 on the 3 methyl groups and a single isolated C−H stretching mode along the z axis. This isolated mode is $\nu_3(a_1)$ at 2892.1 cm^{-1} based mainly on the previous work of McKean et al.,[33] who found a deuterium-isolated C−H mode in $(CD_3)_3CH$ at 2894.1 cm^{-1}.

It is customary to symmetrize the three C−H bond stretches in each methyl group (C_{3v} local symmetry) as r^+ (symmetric stretch, a_1) and r^- (asymmetric stretch, e) and further label the e components as r_a^- (oscillating dipole in a symmetry plane of isobutane) and r_b^- (oscillating dipole perpendicular to a symmetry plane of isobutane). There are three equivalent methyl groups in isobutane, so symmetrizing again gives r^+ (a_1 and e), r_a^- (a_1 and e), and r_b^- (a_2 and e). Looking at the motion vectors from the harmonic calculation, the 10 C−H fundamental modes are $\nu_1(a_1, r_a^-)$, $\nu_2(a_1, r^+)$, $\nu_3(a_1$, C−H isolated), $\nu_9(a_2, r_b^-)$, $\nu_{13}(e, r_b^-)$, $\nu_{14}(e, r_a^-)$, and $\nu_{15}(e, r^+)$.

Table 4. Fitted Spectroscopic Constants for the ν_5 and ν_4 Bands in Units of cm^{-1} with One Standard Deviation in the Last Digits Given in Parentheses

	ground state[a]	$\nu_5(a_1)$	$\nu_4(a_1)$
origin	0	1396.54741(76)	1478.20363(41)
B	[0.259826622][b]	0.2590976(31)	0.2619155(65)
$D_J \times 10^7$	[2.12041]	2.739(23)	7.911(238)
$D_{JK} \times 10^7$	[−3.1314]	[−3.1314]	−10.561(302)
$H_J \times 10^{10}$	[2.676]	[2.676]	4.242(239)
$H_{JK} \times 10^9$	[−1.126]	[−1.126]	−0.090532(4697)
$H_{KJ} \times 10^9$	[1.491]	[1.491]	1.8385(372)
$\sigma_{r.m.s.}$		0.0092	0.0025
number of lines		405	322

[a]Ground-state spectroscopic constants are taken from ref 13. [b]Parameters in square brackets were not fitted.

The r^- modes are highest in frequency, and the two most intense bands are predicted to be $\nu_1(a_1, r_a^-)$ and $\nu_{13}(e, r_b^-)$. They are also predicted to be close in frequency, and two strong features are observed (Figure 1) at 2967.0 and 2968.8 cm^{-1}, tentatively assigned as $\nu_{13}(e, r_b^-)$ and $\nu_1(a_1, r_a^-)$, respectively. These assignments could be switched, and it is useful to remember that for certain values of ς, perpendicular modes can appear to have the same band shape as parallel modes.

The remaining C−H fundamental with a_1 symmetry is $\nu_2(a_1, r^+)$, which is predicted to be moderately strong and should have a strong, clear Q-branch. The only feature in our spectrum (Figure 1) that fits this description is at 2916.76 cm^{-1}. The corresponding r^+ e mode is predicted to be relatively strong and at a higher frequency; the feature at 2952.2 cm^{-1} is a reasonable assignment for $\nu_{15}(e, r^+)$.

The remaining C−H fundamental with e symmetry is $\nu_{14}(e, r_a^-)$, which is predicted to be weaker than $\nu_{15}(e, r^+)$ and to a slightly higher frequency. Based on the intensity, a weak feature at 2944.6 cm^{-1} is a potential assignment. A number of features remain without clear assignments, notably at 2872.4, 2880.2, and 2900.5 cm^{-1}, likely associated with CH_2 overtone and combination modes in Fermi resonance with C−H modes.

LOCAL MODE ANALYSIS

It is interesting to compare the above results to the results of the model calculations shown in Figure 6. We performed three calculations. In the first calculation, shown in Figure 6a, all of the couplings between the methyl groups, as well as the couplings to the lone CH stretch, are set to zero. We call this the decoupled methyl model. This model yields a spectrum that can be assigned and yet includes the important Fermi couplings (Table 5). In Figure 6b and Table 6, we show the local mode model results.[28] The features in the observed spectrum that best match the calculations are included in the last column of Table 6. In Figure 6c, we show results with an additional scaling of the couplings between the CH stretches

DOI: 10.1021/acs.jpca.9b03321
J. Phys. Chem. A 2019, 123, 6185−6193

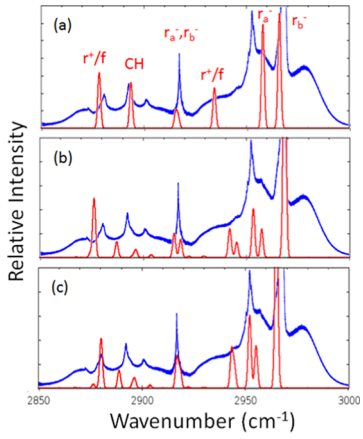

Figure 6. Comparison of experimental (blue, from Figure 1) and local mode model (red) results. (a) Spectra of the decoupled methyl model in which methyl groups and lone CH are decoupled from one another; (b) local mode results with standard scalings; (c) same as (b) but with couplings between CH stretches on the same methyl reduced by 20%.

Table 5. Results of the Uncoupled Methyl Group Local Mode Model[a]

energy (cm^{-1})	intensity (km mol^{-1})	label
2878.4	20.342	$e_x r^+/f$
2878.4	20.343	$e_y r^+/f$
2878.4	6.419	$a_1 r^+/f$
2893.9	38.595	CH
2915.6	0.782	$e_x r_a^-/f$
2915.6	0.782	$e_y r_a^-/f$
2915.6	11.738	$a_1 r_a^-/f$
2916.8	0	$a_2 r_b^-/f$
2916.8	4.73	$e_x r_b^-/f$
2916.8	4.73	$e_y r_b^-/f$
2934.5	12.908	$e_x r^+$
2934.5	12.908	$e_y r^+$
2934.5	8.831	$a_1 r^+$
2958.1	11.715	$e_x r_a^-$
2958.1	11.719	$e_y r_a^-$
2958.2	65.131	$a_1 r_a^-$
2966.2	0	$a_2 r_b^-$
2966.2	49.136	$e_x r_b^-$
2966.2	49.141	$e_y r_b^-$

[a]The f designation describes the lower-energy state of the CH stretch/scissor pair.

on the same methyl groups. Table 6 also gives the eigenstates in terms of a basis whose functions are the eigenfunctions of the uncoupled methyl model of Table 5. We chose this representation because the Fermi couplings are larger than the quadratic couplings between methyl groups.

The decoupled methyl model results of Figure 6a and Table 5 show six transitions. They occur at 2878, 2984, 2916/2917, 2934, 2958, and 2966 cm^{-1}. In this uncoupled limit, the states of three methyl groups are degenerate. We assigned the states based on the eigenstate decomposition of the model eigenstates. For example, the CH stretch components of the three highest-energy transitions written in terms of the CH stretch basis $|n_1 n_2 n_3\rangle$ of the methyl group of Figure 3 with H atoms 1, 2, and 3 are

$$|\Psi^{r^+}\rangle = .29|100\rangle + .48|010\rangle + .29|001\rangle + \cdots$$

$$|\Psi^{r_a^-}\rangle = .47|100\rangle - .64|010\rangle + .47|001\rangle + \cdots$$

$$|\Psi^{r_b^-}\rangle = .67|100\rangle - .67|001\rangle + \cdots$$

The transitions to the Fermi pair of states between the symmetric CH_3 stretch and scissor overtones, denoted r^+/f, occur at 2878/2934 cm^{-1}. The Fermi pair of transitions at 2926/2958 cm^{-1} is labeled r_a^-. The transitions at 2927/2966, which are also a Fermi pair, are labeled r_b^-. The lone CH stretch is observed at 2994 cm^{-1}.

The spectral results in this frequency window are similar to experimental and model results for diphenylethane (Ph_2–CH–CH_3) and deuterated ethyl benzene (Ph–CD_2–CH_3). The former molecule, which also has a lone CH stretch, has transitions at 2882, 2893, 2919, 2941, 2972, and 2975 cm^{-1}. The model predicts transitions at 2882, 2895, 2919/2920, 2942, 2974, and 2977 cm^{-1}.[31]

When the full coupling of the local mode model is considered, the triplet sets of transitions observed in Figure 6a split into a and e components in Figure 6b. The r_b^- state at 2966 cm^{-1} splits into states at 2958 and 2969 cm^{-1} with a_2 and e symmetries, respectively. The state, labeled as r_a^- at 2958, splits into states at 2958 and 2969 cm^{-1} with e and a_1 symmetries, respectively. Consequently, one finds substantial intensity due to the triplet of states at 2969 cm^{-1}. The r^+/f state at 2934 cm^{-1} when there is no coupling splits into states at 2942 and 2953 cm^{-1} with e and a symmetries, respectively. However, these states are quite mixed. Calculated a states at 2918, 2943, and 2953 cm^{-1} all have a substantial r^+/f character. Interestingly, the CH stretch shifts from 2894 to 2887 cm^{-1} with a corresponding factor of 4 drop in intensity. This result is due to the V_{AC} and more importantly the V_{BC} quadratic couplings. The dipoles of the lone CH stretch and the symmetric r^+ mode point in opposite directions, and hence, any coupling between these modes has a substantial effect on the intensity.

In comparing the model results to the experimental spectrum, we find a good match between theory and experiment. The spectral region that is least well described is the lowest-frequency region where the model transition frequencies are slightly lower than those of experiment. To explore how a model parameter might be altered to improve the result, we have decreased the spread in frequency by decreasing the coupling between the CH stretches on the same methyl group by 20%. These V_{AB} and V_{BB} terms are the only ones in the Hamiltonian where a small adjustment improves the agreement. The results, which are improved at the low end of the spectrum, are shown in Figure 6c. This improvement comes at the expense that the transition at the highest-frequency region is now slightly too low compared to that of experiment. One could try for further improvements, but it is already clear that all of the major spectral features can be identified. With a model this simple, we do not expect more. We also note that the largest difference between the CCSD(T) results and density functional results, shown in Table 1, for the off-diagonal terms is the larger V_{AB} and V_{BB} couplings predicted by the higher-level theory. We decreased the values of these terms to improve the results in Figure 6c. Perhaps, higher-order couplings lead to an effective Hamiltonian with smaller V_{AB} and V_{BB} couplings than those predicted at the harmonic level. These changes highlight how small differences

DOI: 10.1021/acs.jpca.9b03321
J. Phys. Chem. A 2019, 123, 6185–6193

Table 6. Energies and Intensities of the Local Mode Model with Eigenstate Labels of the Leading Components Given for a Basis Defined in Table 5[a]

energy (cm^{-1})	intensity (km mol^{-1})	coef	label	coef	label	obs (cm^{-1})
2876.4	18.5	0.97	$e_x,r^+/f$			2880.2
2876.4	18.5	0.97	$e_y,r^+/f$			2880.2
2887.3	9.8	0.9	CH	0.31	$a_1,r_a^-/f$	2992.1
2915.1	15.1	−0.48	a_1,r^+	0.45	$a_1,r_a^-/f$	2916.76
2918.2	5.7	0.59	$e_y,r_a^-/f$			2916.76?
2918.2	5.7	0.59	$e_x,r_a^-/f$			2916.76?
2941.9	8.4	0.76	e_x,r^+			2944.6
2941.9	8.4	0.76	e_y,r^+			2944.6
2945.4	4.7	0.42	$e_y,r_b^-/f$			2945.7?
2945.4	4.7	0.42	$e_x,r_b^-/f$			2945.7?
2953.4	30.5	0.56	a_1,r^+			2952.2
2957.5	8.9	0.97	e_x,r_a^-			2957.3?
2957.5	8.9	0.97	e_y,r_a^-			2957.3?
2968.6	49.3	0.98	e_x,r_b^-			2967.0?
2968.6	49.3	0.98	e_y,r_b^-			2967.0?
2968.6	70.2	−0.91	a_1,r_a^-			2968.8?

[a]The basis functions used in the local mode model are the eigenfunctions of the uncoupled methyl model. The corresponding labels, shown above, refer to the eigenstates reported in Table 5.

in couplings affect the spectrum and highlight the accuracy and limitation of the model.

CONCLUSIONS

New high-resolution infrared spectra[10,11] of isobutane have been analyzed. Rotational analysis of two of the parallel modes has been carried out: $\nu_5(a_1)$ with an origin at 1396.54741(76) cm^{-1} and $\nu_4(a_1)$ at 1478.20363(41) cm^{-1}. Vibrational mode assignments were made with the help of ab initio calculations (Table 3). The C−H stretching region is very perturbed by resonances with the overtone and combination modes of the CH_2 scissor modes. To help understand the vibrational character of the C−H stretches, a local mode analysis was carried out for the 10 C−H stretches and the 9 combinations and overtones of the CH_2 scissor modes. These resonances cause extra bands to appear and shift the modes from their expected positions. For example, the features at 2917 and 2952 cm^{-1} are assigned based on the ab initio calculations (Table 3) as $\nu_2(a_1, r^+)$ and $\nu_{15}(e, r^+)$, respectively. However, the local mode calculations suggest that Fermi resonance gives two a_1 r^+ bands (Table 6, 2915 and 2953 cm^{-1}) and two e r^+ bands (Table 6, 2876 and 2942 cm^{-1}), which match features at 2818, 2952, 2880.2, and 2944.6 cm^{-1} (Table 6, last column), respectively. The local mode calculations are a better match for the observed spectrum. The assignments in Table 3 generally (but not always) agree with those in Table 6.

ASSOCIATED CONTENT

Supporting Information

The Supporting Information is available free of charge on the ACS Publications website at DOI: 10.1021/acs.jpca.9b03321.

PGOPHER-nu4 (TXT)
PGOPHER-nu5 (TXT)

AUTHOR INFORMATION

Corresponding Author

*E-mail: pbernath@odu.edu.

ORCID

Peter F. Bernath: 0000-0002-1255-396X

Notes

The authors declare no competing financial interest.

ACKNOWLEDGMENTS

Funding was provided by the NASA Planetary Data Archiving and Restoration Tool (PDART) program through the grant NNX16AG44G. The authors thank Dan Hewett and Brant Billinghurst for help with the isobutane spectra. E.L.S. gratefully acknowledges support via Grant No. CHE-1566108.

REFERENCES

(1) Pozzer, A.; Pollmann, J.; Taraborrelli, D.; Jöckel, P.; Helmig, D.; Tans, P.; Hueber, J.; Lelieveld, J. Observed and simulated global distribution and budget of atmospheric C_2-C_5 alkanes. *Atmos. Chem. Phys.* **2010**, *10*, 4403−4422.

(2) Grant, A.; Yates, E. L.; Simmonds, P. G.; Derwent, R. G.; Manning, A. J.; Young, D.; Shallcross, D. E.; O'Doherty, S. A five year record of high-frequency in situ measurements of non-methane hydrocarbons at Mace Head, Ireland. *Atmos. Meas. Tech.* **2011**, *4*, 955−964.

(3) Gilman, J. B.; Lerner, B. M.; Kuster, W. C.; De Gouw, J. Source signature of volatile organic compounds from oil and natural gas operations in northeastern Colorado. *Environ. Sci. Technol.* **2013**, *47*, 1297−1305.

(4) Dobrijevic, M.; Loison, J.; Hickson, K.; Gronoff, G. 1D-coupled photochemical model of neutrals, cations and anions in the atmosphere of Titan. *Icarus* **2016**, *268*, 313−339.

(5) Moses, J. I.; Bézard, B.; Lellouch, E.; Gladstone, G. R.; Feuchtgruber, H.; Allen, M. Photochemistry of Saturn's atmosphere: I. Hydrocarbon chemistry and comparisons with ISO observations. *Icarus* **2000**, *143*, 244−298.

(6) Nixon, C. A.; Jennings, D. E.; Flaud, J. M.; Bézard, B.; Teanby, N. A.; Irwin, P. G. J.; Ansty, T. M.; Coustenis, A.; Vinatier, S.; Flasar, F. M. Titan's prolific propane: The Cassini CIRS perspective. *Planet. Space Sci.* **2009**, *57*, 1573−1585.

(7) Greathouse, T. K.; Lacy, J. H.; Bézard, B.; Moses, J. I.; Richter, M. J.; Knez, C. The first detection of propane on Saturn. *Icarus* **2006**, *181*, 266−271.

(8) Durig, J. R.; Wang, A.; Beshir, W.; Little, T. S. Barrier to asymmetric internal rotation, conformational stability, vibrational spectra and assignments, and ab Initio calculations of *n*-butane-d0, d5 and d10. *J. Raman Spectrosc.* **1991**, *22*, 683−704.

DOI: 10.1021/acs.jpca.9b03321
J. Phys. Chem. A 2019, 123, 6185−6193

(9) Lide, D. R., Jr. Structure of the isobutane molecule; change of dipole moment on isotopic substitution. *J. Chem. Phys.* **1960**, *33*, 1519−1522.
(10) Hewett, D. M.; Bernath, P. F.; Billinghurst, B. E. Infrared absorption cross sections of isobutane with hydrogen and nitrogen as broadening gases. *J. Quant. Spectrosc. Radiat. Transfer* **2019**, *227*, 226−229.
(11) Hewett, D. M.; Bernath, P. F.; Wong, A.; Billinghurst, B. B.; Zhao, J.; Lombardo, N. A.; Nixon, C. A.; Jennings, D. E. N_2 and H_2 broadened isobutane infrared absorption cross sections and butane upper limits on Titan. *Icarus*, submitted for publication, 2019.
(12) Lide, D. R., Jr.; Mann, D. Microwave spectra of molecules exhibiting internal rotation. IV. Isobutane, tertiary butyl fluoride, and trimethylphospine. *J. Chem. Phys.* **1958**, *29*, 914−920.
(13) Priem, D.; Colmont, J.-M.; Petitprez, D.; Bailleux, S. The rotational spectrum of isobutane up to 640 GHz: splitting of the |K| = 3 transitions. *J. Mol. Spectrosc.* **1997**, *184*, 84−87.
(14) Hilderbrandt, R.; Wieser, J. The zero point average structure of isobutane as determined by electron diffraction and microwave spectroscopy. *J. Mol. Struct.* **1973**, *15*, 27−36.
(15) Pitzer, K. S.; Kilpatrick, J. E. The entropies and related properties of branched paraffin hydrocarbons. *Chem. Rev.* **1946**, *39*, 435−447.
(16) Evans, J.; Bernstein, H. The vibrational spectra of isobutane and isobutane-d1. *Can. J. Chem.* **1956**, *34*, 1037−1045.
(17) Wilmshurst, J.; Bernstein, H. The infrared and Raman spectra of $HC(CD_3)_3$ and $DC(CD_3)_3$. *Can. J. Chem.* **1957**, *35*, 969−979.
(18) Schachtschneider, J. H.; Snyder, R. G. Vibrational analysis of the n-paraffins—II: Normal co-ordinate calculations. *Spectrochim. Acta* **1963**, *19*, 117−168.
(19) Weiss, S.; Leroi, G. E. Infrared spectra and internal rotation in propane, isobutane and neopentane. *Spectrochim. Acta, Part A* **1969**, *25*, 1759−1766.
(20) Manzanares, C.; Peng, J.; Mina-Camilde, N.; Brock, A. Overtone spectroscopy of isobutane at cryogenic temperatures. *Chem. Phys.* **1995**, *190*, 247−259.
(21) Hassoon, S.; Snavely, D. L. Hot bands in overtone absorption of pyrrole, methyl isocyanide and isobutane: Photoacoustic spectra at 140 °C. *J. Chem. Phys.* **1993**, *99*, 2511−2519.
(22) Schrader, B.; Pacansky, J.; Pfeiffer, U. Calculation of the frequencies and intensities in the infrared spectra of matrix-isolated tert-butyl radical and isobutane. *J. Phys. Chem. A* **1984**, *88*, 4069−4073.
(23) Petrov, D.; Matrosov, I.; Zaripov, A. Raman spectra of *n*-butane, isobutane, *n*-pentane, and isopentane in a methane environment. *Opt. Spectrosc.* **2018**, *125*, 5−9.
(24) Mirkin, N.; Krimm, S. Ab initio analysis of the vibrational spectra of conformers of some branched alkanes. *J. Mol. Struct.* **2000**, *550*−*551*, 67−91.
(25) Pele, L.; Šebek, J.; Potma, E. O.; Gerber, R. B. Raman and IR spectra of butane: Anharmonic calculations and interpretation of room temperature spectra. *Chem. Phys. Lett.* **2011**, *515*, 7−12.
(26) MacPhail, R.; Strauss, H.; Snyder, R.; Elliger, C. Carbon-hydrogen stretching modes and the structure of n-alkyl chains. 2. Long, all-trans chains. *J. Phys. Chem. A* **1984**, *88*, 334−341.
(27) Hewett, D. M.; Bocklitz, S.; Tabor, D. P.; Sibert, E. L., III; Suhm, M. A.; Zwier, T. S. Identifying the first folded alkylbenzene via ultraviolet, infrared, and Raman spectroscopy of pentylbenzene through decylbenzene. *Chem. Sci.* **2017**, *8*, 5305−5318.
(28) Tabor, D. P.; Hewett, D. M.; Bocklitz, S.; Korn, J. A.; Tomaine, A. J.; Ghosh, A. K.; Zwier, T. S.; Sibert, E. L., III Anharmonic modeling of the conformation-specific IR spectra of ethyl, *n*-propyl, and *n*-butylbenzene. *J. Chem. Phys.* **2016**, *144*, No. 224310.
(29) Sharpe, S. W.; Johnson, T. J.; Sams, R. L.; Chu, P. M.; Rhoderick, G. C.; Johnson, P. A. Gas-phase databases for quantitative infrared spectroscopy. *Appl. Spectrosc.* **2004**, *58*, 1452−1461.
(30) Frisch, M. J.; Trucks, G. W.; Schlegel, H. B.; Scuseria, G. E.; Robb, M. A.; Cheeseman, J. R.; Scalmani, G.; Barone, V.; Petersson, G. A.; Nakatsuji, H. et al. *Gaussian 09*; Gaussian, Inc.: Wallingford CT, 2016.
(31) Sibert, E. L.; Tabor, D. P.; Kidwell, N. M.; Dean, J. C.; Zwier, T. S. Fermi resonance effects in the vibrational spectroscopy of methyl and methoxy groups. *J. Phys. Chem. A* **2014**, *118*, 11272−11281.
(32) Western, C. M. PGOPHER: A program for simulating rotational, vibrational and electronic spectra. *J. Quant. Spectrosc. Radiat. Transfer* **2017**, *186*, 221−242.
(33) McKean, D. C.; Biedermann, S.; Bürger, H. CH bond lengths and strengths, unperturbed CH stretching frequencies, from partial deuteration infrared studies: t-butyl compounds and propane. *Spectrochim. Acta, Part A* **1974**, *30*, 845−857.

DOI: 10.1021/acs.jpca.9b03321
J. Phys. Chem. A 2019, 123, 6185−6193